Accepted Manuscript

Photocatalytic oxidation of aromatic alcohols over silver supported on cobalt oxide nanostructured catalyst

Xianbing Ji, Yinxia Chen, Bappi Paul, S. Vadivel

PII: S0925-8388(18)34869-2

DOI: https://doi.org/10.1016/j.jallcom.2018.12.307

Reference: JALCOM 48950

To appear in: *Journal of Alloys and Compounds*

Received Date: 24 September 2018

Revised Date: 24 December 2018

Accepted Date: 26 December 2018

Please cite this article as: X. Ji, Y. Chen, B. Paul, S. Vadivel, Photocatalytic oxidation of aromatic alcohols over silver supported on cobalt oxide nanostructured catalyst, *Journal of Alloys and Compounds* (2019), doi: https://doi.org/10.1016/j.jallcom.2018.12.307.

This is a PDF file of an unedited manuscript that has been accepted for publication. As a service to our customers we are providing this early version of the manuscript. The manuscript will undergo copyediting, typesetting, and review of the resulting proof before it is published in its final form. Please note that during the production process errors may be discovered which could affect the content, and all legal disclaimers that apply to the journal pertain.

Graphical abstract

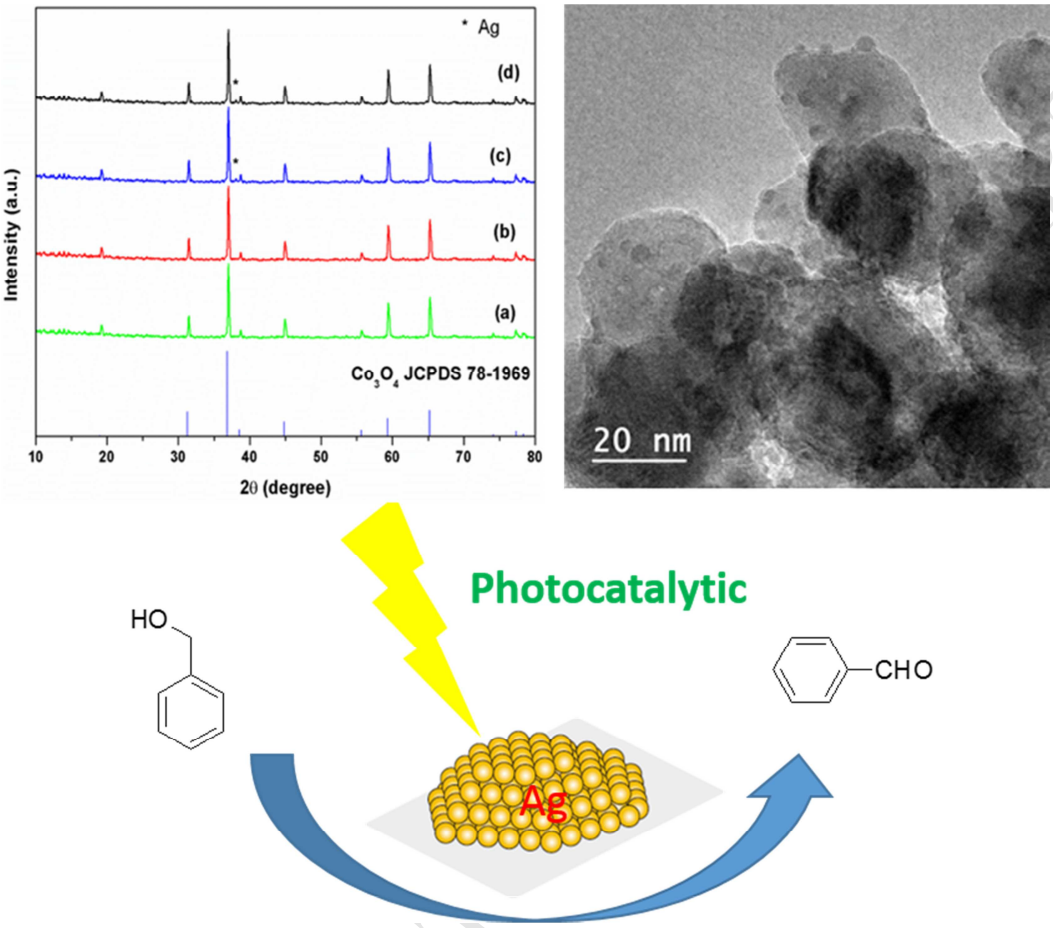

ACCEPTED MANUSCRIPT

ACCEPTED MANUSCRIPT

Photocatalytic oxidation of aromatic alcohols over silver supported on cobalt oxide nanostructured catalyst

Xianbing Ji[a], Yinxia Chen[a]*, Bappi Paul[b]*, S. Vadivel[c]

[a]Hebei University of Environmental Engineering, Qinhuangdao, Hebei-066102, China

[b]Department of Chemistry, National Institute of Technology Silchar, Silchar-788010, Assam, India

[c]Department of Chemistry, PSG College of Technology, Coimbatore 641004, India

*Corresponding authors. Tel: +91-03842-242915; fax: +91-03842-224797

Email: chyxsd@126.com (Y. Chen); bappipaulnits@gmail.com (B. Paul)

ABSTRACT

In this paper, we report an in-situ synthesis of silver supported on cobalt oxide (Ag/Co_3O_4) nanoparticles (NPs) and studied the catalytic activity of this material as an eco-friendly, simple, recyclable and efficient catalyst for one-pot photocatalytic oxidation of aromatic alcohols. Ag nanoparticles with the sizes of 2–5 nm supported on spherical Co_3O_4 with the radius between 40 and 60 nm were synthesized by homogeneous chemical precipitation followed by hydrothermal heating. The as-synthesized catalyst was thoroughly characterized by powder X-ray diffraction (XRD), scanning electron microscopy (SEM), energy-dispersive X-ray spectroscopy (EDX), elemental mapping, transmission electron microscopy (TEM), X-ray photoelectron spectroscopy (XPS), Fourier transform infrared spectroscopy (FTIR), thermogravimetric analysis (TGA) and N_2 adsorption-desorption isotherm (BET) analysis. It was observed that the catalysts with 1 wt% of silver loading shows high activity and selectivity toward the target aldehyde product. The effects of different reaction parameters such as reaction time, oxidant and solvent were investigated and studied in detail. The synergistic effect between the surface Ag NPs and Co_3O_4 nanospheres plays a vital role toward very high catalytic activity.

Keywords: Oxide materials; Chemical synthesis; Catalysis; X-ray diffraction

1. Introduction

During last few decades, preparation and characterization of inorganic materials with nanosized dimensions and morphological specificity has become highly important and received a great deal of interest in various science and technology fields [1-7]. Recently, nanomaterials have attracted much research attention due to their applications in medicine, biology, electronics and chemical industries [8-11]. Nanostructured materials with low density and high specific surface area are considered suitable candidates for a variety of applications. Their significantly enhanced activity can be attributed to their highly accessible surface area with a large number of active sites [12,13]. It was observed that nanomaterials doped with another metal boost their catalytic efficiency to great extent due to synergistic effects [14]. Noble metal nanomaterials such as silver and gold have shown tremendous potential for applications in various fields including catalysis [15, 16]. Their controlled effect as dopants on various transition and nontransition metal oxide supports, such as titania, alumina, and silica, has provided a new aspect to their utility in catalytic science and technology [17-21]. Several green methods for the synthesis of Ag nanoparticles (NPs) are known [22]. Synthesis methods for supported transition metal oxide nanomaterials such as sonochemical methods, microwave irradiation, and vapor deposition have been studied and they have their own advantages and disadvantages. Despite significant research efforts, controlled and easy synthesis of Ag-supported Co_3O_4 nanomaterials in solution is still highly challenging. Development of a facile method for the synthesis of Ag-supported Co_3O_4 nanomaterials with desired size, shape and morphology is still considered a challenging task. Huang *et al* has synthesized Ag-decorated Co_3O_4 nanosheets on nickel foam *via* a hydrothermal method and it was found that the morphology of Co_3O_4 can be controlled by adjusting the hydrothermal time and the concentration of reactants [5]. Herein, we report a

simple and reproducible preparation method for the synthesis of silver supported on Co_3O_4 spinel nanoparticles *via* a hydrothermal synthesis followed by calcination. Silver supported on Co_3O_4 nanoparticles was synthesized by an in-situ synthesis procedure and it was found that the in-situ synthesis procedure is better than the impregnation method for the photocatalytic oxidation of alcohol. The added advantage of the synthesis procedure is that it can be applied on a large scale synthesis (up to 10 g).

Oxidation of alcohols is one of the most important transformations in synthetic organic chemistry [23, 24]. The oxidation products are known to be essential intermediates in the manufacture of agrochemicals, fine chemicals, pharmaceuticals and high-value commodity chemicals [25, 26]. With a growing concern with economic and environmental acceptability, researchers across the world are devoting much effort to accomplish such oxidation with oxygen or hydrogen peroxides [27-30]. Several excellent catalysts have been developed for environmentally benign oxidation of alcohols to carbonyl compounds [31]. Recently, photocatalytic oxidation of aromatic alcohols where aldehyde was obtained as a major product using a nanostructured catalyst has been of interest among researchers [32-35]. In particular, Jing *et al.* have reported on the use of Bi_2MoO_6 spheres for the photocatalytic oxidation of benzyl alcohol [36]. Zhang *et al.* have reported on the photocatalytic oxidation of benzyl alcohol over TiO_2 nanorods loaded with Au-Pt nanoparticles. They have immobilized the Au-Pt nanoparticles on TiO_2 nanorods where photocatalytic activity for benzyl alcohol was obtained under visible light irradiation [37]. Perovskite materials were also studied for the selective photocatalytic oxidation of benzylic alcohols [38]. Ziarati *et al* has synthesized graphene highly wrapped yolk@shell TiO_2 (G-HW-Y@S-TiO2) nanomaterials for photocatalytic performance in visible light oxidation of aromatic alcohols and found that the selectivity of aldehyde was intact even after 12 h of reaction [39]. Ding *et al* has reported graphitic C_3N_4-based polymers for photocatalytic oxidation of aromatic

alcohols. The study reveals that vacancy defect in the semiconductors plays an important role in enhancing the photocatalytic activity of semiconductor photocatalysts [40]. Qiu *et al* has studied noble metal nanoparticle-functionalized Zr-metal organic frameworks for aromatic oxidation of alcohols to aldehydes. It was observed that the photocatalytic oxidation of aromatic alcohols to aldehydes was enhanced over Au/UiO-66-NH_2 or Au/UiO-66 photocatalyst, but the activity was suppressed over Pt loading [41]. All the materials have their own advantage and disadvantage. Moreover all the reported process uses an atom-economic catalyst system that utilizes available green and clean renewable solar energy which is favorable from an environmental standpoint. However some suffers from multi-step catalyst synthesis procedure, long reaction run, low conversion or low selectivity. Therefore, we herein report a simple single step procedure for the synthesis of silver supported on Co_3O_4 spinel nanoparticles and studied its activity for environmentally friendly photocatalytic oxidation of aromatic alcohols. It was found that the synthesized nanomaterials is highly active for photocatalytic oxidation of aromatic alcohols and a small loading of silver is sufficient for high conversion and selectivity towards the target product aldehyde.

2. Experimental

2.1 Catalyst preparation

A spherical Ag/Co_3O_4 spinel nanoparticles catalyst was prepared by surfactant-assisted hydrothermal method through the modification of a synthesis method previously reported by us [42]. The benefit of this procedure is that the catalyst can be synthesized on a large scale (up to 10 g) and in a highly reproducible manner. First, 11.96 g of $Co(NO_3)_2{\cdot}6H_2O$ and 0.16 g of $AgNO_3$ were dissolved separately in a minimum volume of distilled water. The resultant solutions were then mixed and stirred magnetically. Subsequently, 1.8 g CTAB dissolved in a mixture of 50 ml distilled water and 2 ml ethanol was added to the mixed solution. Through the gradual

addition of an ammonia solution, the pH of the solution was adjusted to 8 followed by the addition of 0.1 g of hydrazine and was finally stirred for another 20 min at which point the mixture turned into a homogeneous solution with a jet black color. Then, the precursor solution was transferred into a 50 mL autoclave with a Teflon liner and was held at 180 °C for 12 h. After washing with excess H_2O and ethanol, the obtained sample was dried at 80 °C for 12 h. The as-obtained precursor powder was then calcined in a quartz reactor inside a tubular resistance furnace for 4 h at 550 °C to obtain the Ag/Co_3O_4 spinel nanoparticles catalyst powder. The catalyst was also prepared by the impregnation method and the coprecipitation method. The loading of the silver nanoparticles was confirmed by inductively coupled plasma atomic emission spectrometer analysis (ICP-AES).

2.2 Photocatalytic oxidation of alcohol

Liquid phase photocatalytic alcohol oxidation was performed in a 100 mL quartz reactor equipped with magnetic stirrer with O_2 atmosphere under simulated sunlight irradiation. The 20 mg of photocatalyst was suspended in 10 ml acetonitrile, used as a solvent, followed by the addition of aromatic alcohol (1 mmol). The reaction was performed under the irradiation of a 300 W Xe lamp without UV and IR cut-off filters. At regular intervals of the photooxidation reaction, a small portion of the sample was withdrawn from the reaction mixture for analysis. The conversion and selectivity of the product were calculated by gas chromatography (GC, Agilent 7890) using methylbenzene as an external standard.

3. Results and discussion

<Fig. 1>

The phase purity and crystalline structure of Ag/Co_3O_4 was investigated using powder X-ray-diffraction (PXRD) analysis. The powder XRD patterns of the synthesized

silver supported by Co_3O_4 nanoparticles are presented in Fig. 1. The peaks at 2θ of 19.0°, 31.2°, 36.9°, 44.8°, 55.7°, 59.3°, 65.3°, 74.1° and 77.3° confirmed the formation of the face-centered cubic structured Co_3O_4 nanoparticles. The diffraction pattern matched the reported Co_3O_4 patterns well (JCPDS 78-1969). No crystalline phase of metallic Ag was detected by XRD for 0.5% and 1% Ag/Co_3O_4 (Fig. 1(a and b)), indicating that the very small Ag-crystallites are highly dispersed over the Co_3O_4 support. Moreover, in addition to the diffraction peaks of Co_3O_4, we observed an additional peak at 2θ of 38.1° corresponding to the metallic Ag crystal faces of (111) which coincide well with the literature values (JCPDS File no. 89-3722) for 1.5% Ag/Co_3O_4 and the spent catalyst (Figs. 1(c,d)). No impurity peaks were observed, indicating the high purity of the nanoparticles. No change in the XRD pattern of the spent catalyst was observed even after five cycles of reuse (Fig. 1(d)).

<Fig. 2>

The morphology of the as-prepared Ag/Co_3O_4 catalysts was determined by scanning electron microscopy. The representative SEM images of the fresh catalyst show an almost spherical shape with the size of 40-60 nm (Figs. (2(a,b). The EDS pattern showed only the presence of cobalt, silver and oxygen and no impurities could be observed in the spectra (Fig. 2(d)). The dispersion of silver on the nanocrystalline Co_3O_4 was confirmed by the elemental mapping of the catalyst that found a homogenous distribution of Ag on the nanocrystalline Co_3O_4 support (Fig. 3). The spent catalyst also showed a homogenous distribution (Fig. S2 in ESI).

<Fig. 3>

<Fig. 4>

High-resolution transmission electron microscopy (HRTEM) analysis was carried out to examine the particle size and distribution of the silver nanoparticles on nanocrystalline Co_3O_4 (Fig. 4). The TEM image of Co_3O_4 nanoparticles showed an almost spherical shape with the size of 40-60 nm. The average particle size of silver nanoparticles was observed in the range of 2–5 nm. The spacing of the lattice fringes was found to be 0.28 nm and 0.23 nm, possibly due to the (220) plane of Co_3O_4 and the (111) plane of metallic Ag, respectively. Furthermore, the TEM image of the spent catalyst (Fig. S1 in ESI) shows almost the same shape and size even after five reuses. The corresponding particle size distribution histogram of the Ag nanoparticles showed a very narrow particle size distribution with the sizes between 2 and 5 nm which is in good agreement with the values obtained from the XRD data (Fig. S1 in ESI).

<Fig. 5>

The metallic state and the surface composition of the synthesized nanospheres were investigated by X-ray photoelectron spectroscopy (XPS). As shown in Fig. 5, the XPS spectrum of the samples reveals the presence of the Ag, Co, and O elements. The Co 2p spectrum of the fresh catalyst could be fitted to two spin-orbit doublets that are characteristic of Co^{2+} and Co^{3+} and two shake-up satellites. The two main peaks at 780.1 and 795.2 eV with a characteristic peak difference of 15.1 eV can be assigned to the $2p_{3/2}$ and $2p_{1/2}$ of Co^{2+} and Co^{3+}, respectively (Fig. 5(a))[43]. The O 1s spectra of the fresh catalyst could be deconvoluted to three different oxygen contribution peaks labeled as O_{latt}, O_{hyd} and O_{ads} at the binding energies of 529.8, 531.8, and 533.2 eV, corresponding to the lattice oxygen, hydroxyl oxygen and physically adsorbed oxygen (O_{ads}), respectively (Fig. 5(b)). The high-resolution spectrum of the silver nanoparticles contained two prominent Ag $3d_{5/2}$ and Ag $3d_{3/2}$ peaks at the binding energies of 368.2 eV and 374.1 eV, corresponding to metallic Ag^0 and the two small peaks at 368.6 and 374.6 eV are ascribed to the Ag^+ species (Fig. 5(c)) [44].

<Fig. 6>

The specific surface area, pore volume and pore diameter play important roles in the catalytic activity. The textural properties of the synthesized Ag/Co_3O_4 nanoparticles were investigated using nitrogen adsorption and desorption isotherms (Fig. 6). The N_2 adsorption–desorption isotherms of the samples show typical IV-type isotherms with high pore volume and specific surface area. The BET surface areas of the as-synthesized nanoparticles and the spent catalyst were measured to be 46.23 and 40.74 m^2g^{-1}, respectively (Fig. 6(a)). The Barrett-Joyner-Halenda (BJH) pore size distribution indicated that most of the pores are in the range from 2 to 15 nm (Fig. 6(b)). Table 1 summarizes the structural and the textural properties such as the surface area, pore volume and pore size derived from the nitrogen adsorption and desorption isotherms of the prepared nanomaterials.

<Table 1>

<Fig. 7>

The surface-coordination of the organic surfactant molecules on the uncalcined nanoparticles was studied by FTIR analysis (Fig. 7). A comparison of the FTIR spectrum of a dried uncalcined nanoparticles precursor with that of the calcined nanoparticles was performed, not only confirming the presence of the surfactant molecules but also revealing the nature of the interaction of the surfactant molecules with the metal oxide surface. For dried uncalcined nanoparticles, the O-H group stretching vibration was observed at 3472 cm^{-1}. The peaks at 1632 cm^{-1} were attributed to the C=O stretching vibration and the peaks at 1382 and 1109 cm^{-1} were due to the C–N vibrational mode, confirming the presence of CTAB in the precursor (Fig. 7(a)). After the sample was washed and calcined, the peak intensity of the calcined nanoparticle decreased with two additional peaks observed at 674 and 569 cm^{-1} that

can be attributed to the characteristic peaks of the metal oxide (Co–O), confirming the removal of the surfactant during the calcination (Fig. 7(b)).

<Fig. 8>

The TGA curve (Fig. 8) shows a two-step decomposition pathway. The weight loss of 4.04% in the first step (30-200°C) is due to the removal of the physically adsorbed moisture in the precursor. The weight loss of 32.16% in the second step (200-520°C) indicated the combustion of CTAB from the surface and the subsequent conversion of $Ag/Co(OH)_3$ to Ag/Co_3O_4.

The UV-visible light absorption properties of the composites were measured by UV-Vis DRS spectroscopy (Fig. S3(a) in ESI). The Ag/Co_3O_4 composites shows a wide absorption range over the visible light region. Band gaps were calculated using the Tauc plot and the band gap of Ag/Co_3O_4 was found to be 1.47 eV (Fig. S3(b) in ESI). Photoluminescence (PL) was also investigated at room temperature, and the Ag/Co_3O_4 composites were excited at the wavelength of 310 nm and the characteristic green emission peak was observed at 492 nm (Fig. S3(c) in ESI).

3.2 Catalytic activity

We have explored the catalytic activity of the synthesized nanomaterial for photocatalytic alcohol oxidation. Various reaction parameters such as the solvent, time and catalyst weight, were optimized in order to obtain the best result, with benzyl alcohols chosen as the standard substrate. The photocatalytic oxidation experiment was conducted under different solvents *viz.* acetonitrile, dimethyl carbonate, trifluorotoluene, tributyl phosphate and water. It was apparent from the optimization experiments that acetonitrile was the best and most suitable solvent for the present photocatalytic reaction (Table 2). Table 3 summarizes the optimized

parameters of various catalyst for the photocatalytic alcohol oxidation where aldehyde was detected as the major product with benzoic acid as a minor product.

<Table 2>

To explore the individual role of the oxide, we have performed the catalytic activity measurements in the presence of commercially available Ag and Co_3O_4 and found a negligible amount of activity. By contrast, when the reaction was performed with the commercially available Ag/Co_3O_4 catalyst, we find an increase in the conversion of the alcohol but the activity of the reported synthesized silver supported on Co_3O_4 is still not comparable. This can be attributed to the small particular size and high surface area which leads to a high dispersion of catalyst compared to the commercial catalyst, which has an irregular shape and large particle size, leading to the limited accessibility of the catalyst for the catalytic reaction. By contrast, the synthesized nanocatalyst consists of highly dispersed nanospheres, leading to more exposed active surface sites for the catalytic reaction to occur. Again, when the reaction was performed in absence of the catalyst and in the presence of the oxidant, we observed a negligible conversion amount, underscoring the vital role of the catalyst in the photocatalytic oxidation reaction of alcohol and for the selectivity to benzaldehyde.

<Table 3>

Taking into account this optimized parameter, we explored the scope of the reaction for various substituted alcohols. It was observed that the substituted electron-donating group facilitates the oxidation reaction, whereas the electron-withdrawing group retards the formation of the aldehyde (Table 4). When the substrate is an electron-donating group such as $-CH_3$ and $-OCH_3$, it facilitates the oxidation reaction with the reaction completed in a short time with a somewhat high conversion. Whereas when the substrate is an electron-

withdrawing group such as Br and F. aldehyde formation is hampered, so that the reaction requires a long time to complete. The conversion and selectivity are not so much affected, however, we have drawn the conclusion with respect to time. Based on the results and previously reported methods, we proposed a possible mechanism as shown in Scheme 1. Under the irradiation of visible light, the photogenerated carriers were produced, the excited electrons migrated from the valence band (VB) of Co_3O_4 to the conduction band (CB). At the same time, the electrons from the conduction band of Co_3O_4 migrated to the Ag nanoparticles where the surface plasmon resonance (SPR) activity of Ag also plays a vital role; the Ag nanoparticle also absorbs photons producing electron-hole pairs due to SPR, leading to the prevention of the electron-hole pair recombination and an excellent photocatalytic activity. The CB energy level of 0.50 V is more positive than the potential of $O_2/{}^{\cdot}O_2^-$ which is -0.046 V so that the electrons transfers to Ag when the O_2 is reduced to ${}^{\cdot}O_2^-$ which in turns produces the superoxide radical (${}^{\cdot}OOH$). The superoxide radical converts the activated alcohol cation radicals produced by the action of h^+ holes in the VB of Co_3O_4 on the alcohol to aldehyde [40,45]. A comparison between the present catalyst and some of the previously reported catalytic methods for the photocatalytic oxidation of benzyl alcohol to benzaldehyde are summarized in table S1 in ESI.

<Table 4>

After each catalytic run and completion of the reaction, the solid catalyst was filtered from the reaction mixture and washed with ethanol, and reused for multiple cycles to check the stability of the catalyst (Fig. 9). Negligible change in the activity of the recovered catalyst after 5 consecutive cycle was observed, indicating the true heterogeneity of the catalyst (Table 2, entry 7). The SEM image of the spent catalyst showed almost similar sizes and shapes to that of the fresh catalyst (Fig. 2(c)). Moreover, a negligible amount of leaching of the metal was detected during the reaction (concentrations of both metals were <2 ppb).

ACCEPTED MANUSCRIPT

<Fig. 9>

4. Conclusions

In summary, we have presented a facile and simple surfactant-assisted synthesis of silver nanoparticles supported on the Co_3O_4 nanoparticles *via* hydrothermal heating followed by calcination. The methodology adopted for the synthesis of the supported nanoparticle is simple and can be readily utilized for large-scale synthesis. Initial characterization shows that the nanoparticle is spherical in shape with the size of 40-60 nm. The synthesized nanoparticle was evaluated as a catalyst for one-pot photocatalytic oxidation of alcohol to aldehyde. The catalyst with 1% Ag loading was found to have the optimum loading for the photocatalytic alcohol oxidation to aldehyde with the high conversion of 76% and aldehyde selectivity of >99% within 8 h of reaction time.

Acknowledgements

The author like to thank the prominent talent project, Hebei university of environmental engineering (BJRC201701), the project of natural science foundation of the Hebei province (E2016415004), the project of science and technology department of the Hebei Province (15213629) and the scientific research project item of the Hebei province education office (QN2016032). We also acknowledge the Qinhuangdao key laboratory of environment functional materials.

References

[1] Y.B. Miao, S.S. Wang, Size- and shape-dependent transformation of nanosized titanate into analogous anatase titania nanostructures, J. Am. Chem. Soc. 128 (2006) 8217-8226.

[2] J. Wang, L. Zhu, X. Zhang, M. Yang Size and shape dependent polarizabilities of sandwich and rice-Ball Co_nBz_m clusters from density functional theory, J. Phys. Chem. A 112 (2008) 8226-8230.

[3] H.L. Sun, H.T. Shi, F. Zhao, L. Qi, S. Ghao, Shape-dependent magnetic properties of low-dimensional nanoscale prussian blue (PB) analogue $SmFe(CN)_6 \cdot 4H_2O$, Chem Commun. 0 (2005) 4339-4341.

[4] S.M. Pourmertazari, M.R. Nasrabadi, M.K. Shalemzari, M.M. Zahedi, S.S. Hajimirsadeghi, I. Omrani, Synthesis, structure characterization and catalytic activity of nickel tungstate nanoparticles, Appl. Surf. Sci. 263 (2012) 745-752.

[5] H. Huanga, S. Luo, C. Liua, Q. Wang, Z. Wang, Y. Zhang, A. Hao, Y. Liu, J. Lia, Y. Zhai, Y. Dai, Ag-decorated highly mesoporous Co_3O_4 nanosheets on nickel foam as an efficient free-standing cathode for Li-O_2 batteries, J. Alloys Compd. 726 (2017) 939-946.

[6] S. Lia, S. Hua , W. Jianga , Y. Liub , Y. Zhoua, Y. Liua , L. Mo, Hierarchical architectures of bismuth molybdate nanosheets onto nickel titanate nanofibers: Facile synthesis and efficient Photocatalytic removal of tetracycline hydrochloride, J. Colloid Interface Sci. 521 (2018) 42-49.

[7] S. Li, S. Hu, W. Jiang, Y Liu, Y. Zhou, J. Liu, Z. Wang, Facile synthesis of cerium oxide nanoparticles decorated flower-like bismuth molybdate for enhanced photocatalytic activity toward organic pollutant degradation, J. Colloid Interface Sci. 530 (2018) 171-178.

[8] J.A. Dahl, B.L.S. Maddux, J.E. Hutchinson, Toward greener nanosynthesis, Chem. Rev. 107 (2007) 2228.

[9] J.E. Hutchinson, Greener nanoscience: A proactive approach to advancing applications and reducing implications of nanotechnology, ACS Nano. 2 (2008) 395-402.

[10] S. Li, X. Shen, J. Liu, L. Zhang, Synthesis of Ta_3N_5/Bi_2MoO_6 core–shell fiber-shaped heterojunctions as efficient and easily recyclable photocatalysts, Environ. Sci.: Nano 4 (2017) 1155-1167.

[11] S. Lia, S. Hu, W. Jiang, Y. Liu, J. Liu, Z. Wang, Facile synthesis of flower-like Ag_3VO_4/Bi_2WO_6 heterojunction with enhanced visible-light photocatalytic activity, J. Colloid Interface Sci. 501 (2017) 156-163.

[12] R.B. Laughlin, Anomalous quantum hall effect: an incompressible quantum fluid with fractionally charged excitations, Phys. Rev. Lett. 50 (1983) 1395.

[13] J. Hu, T.W. Odom, C.M. Lieber, Chemistry and physics in one dimension: synthesis and properties of nanowires and nanotubes, Acc. Chem. Res. 32 (1999) 435-445.

[14] D. Wang, Y. Li, Bimetallic Nanocrystals: liquid-phase synthesis and catalytic applications, Adv. Mater. 23 (2011) 1044-1060.

[15] V.K. Sharma, R.A. Yngard, Y. Lin, Silver nanoparticles: green synthesis and their antimicrobial activities, Adv. Colloid Interface Sci. 145 (2009) 83-96.

[16] B. Paul, B. Bhuyan, D.D. Purkayastha, M. Dey, S.S. Dhar, Green synthesis of gold nanoparticles using pogestemon benghalensis (B) O. Ktz. leaf extract and studies of their photocatalytic activity in degradation of methylene blue, Mater. Lett. 148 (2015) 37-40.

[17] P. Wang, Z. Wang, J. Li, Y. Bai, Preparation, characterizations, and catalytic characteristics of Pd nanoparticles encapsulated in mesoporous silica, Microporous Mesoporous Mater. 116 (2008) 400-405.

[18] S.E. Davis, M.S. Ide, R.J. Davis, Selective oxidation of alcohols and aldehydes over supported metal nanoparticles, Green Chem. 15 (2013) 17-45.

[19] J.M. Xu, J.P.Cheng, The advances of Co_3O_4 as gas sensing materials: A review, J. Alloys Compd. 686 (2016) 753-768.

[20] C. Wen, A. Yin, W.L. Dai, Recent advances in silver-based heterogeneous catalysts for green chemistry processes, Appl. Catal,. B. 160-161 (2014) 730-741.

[21] R. Grabowski, J. Słoczynski, M. Sliwa, D. Mucha, R.P. Socha, M. Lachowska, J. Skrzypek, Influence of polymorphic ZrO_2 phases and the silver electronic state on the activity of Ag/ZrO_2 catalysts in the hydrogenation of CO_2 to methanol, ACS Catal. 1 (2011) 266-278.

[22] M. Cinelli, S.R. Coles, M.N. Nadagouda, J. Błaszczynski, R. Slowinski, R.S. Varma K. Kirwan, A green chemistry-based classification model for the synthesis of silver nanoparticles, Green Chem. 17 (2015) 2825-2839.

[23] R.A. Sheldon, H. Bekkum, Fine chemical through heterogeneous catalysis, Wiley-VCH, Weinheim, 2001 (chapter 9).

[24] H. A. Wittcoff, B.G. Reuben, J.S. Plotkin, Industrial organic chemical, Wiley, New Jersey, 2004.

[25] R.A. Sheldon, J.K. Kochi, Metal-catalyzed oxidations of organic compounds, Academic Press: New York, 1984.

[26] M. Hudlicky, Oxidation in organic chemistry; American Chemical Society: Washington, DC, 1990.

[27] P.P. Hankare, P.D. Kamble, S.P. Maradur, M.R. Kadam, U.B. Sankpal, R.P. Patil, R.K. Nimat, P.D. Lokhande, Ferrospinels based on Cu and Co prepared via low temperature route as efficient catalysts for the selective oxidation of alcohol, J. Alloys Compd. 487 (2009) 730-734.

[28] K. Mori, T. Hara, T. Mizugaki, K. Ebitani, K. Kaneda, Hydroxyapatite-supported palladium nanoclusters: a highly active heterogeneous catalyst for selective oxidation of alcohols by use of molecular oxygen, J. Am. Chem. Soc. 126 (2004) 10657-10666.

[29] R. Wang, B. Li, Y. Xiao, X. Tao, X. Su, X, Dong, Optimizing Pd and Au-Pd decorated Bi_2WO_6 ultrathin nanosheets for photocatalytic selective oxidation of aromatic alcohols, J. Catal. 364 (2018) 154-165.

[30] S.E. Davis, M.S. Ide, R.J. Davis, Selective oxidation of alcohols and aldehydes over supported metal nanoparticles, Green Chem. 15 (2013) 17-45.

[31] L. Chen, J. Tanga, L.N. Song, P. Chen, J. He, C.T. Aub, S.F. Yin, Heterogeneous photocatalysis for selective oxidation of alcohols and hydrocarbons, Appl. Catal., B 242 (2019) 379–388

[32] H. Li, R. Liu, S. Lian, Y. Liu, H. Huang, Z. Kang, Near-infrared light controlled photocatalytic activity of carbon quantum dots for highly selective oxidation reaction, Nanoscale 5 (2013) 3289–3297.

[33] C.A. Unsworth, B. Coulson, V. Chechik, R.E. Douthwaite, Aerobic oxidation of benzyl alcohols to benzaldehydes using monoclinic bismuth vanadate nanoparticles under visible light irradiation: Photocatalysis selectivity and inhibition, J. Catal. 354 (2017) 152–159

[34] E. Safaei, S. Mohebbi, Boosted photocatalytic performance of uniform hetero-nanostructures of Bi_2WO_6/CdS and Bi_2WO_6/ZnS for aerobic selective alcohol oxidation, J. Photochem. Photobiol., A 371 (2019) 173–181

[35] J. Wang, Z. Chen, G. Zhai, Y. Men, Boosting photocatalytic activity of WO_3 nanorods with tailored surface oxygen vacancies for selective alcohol oxidations, Appl. Surf. Sci. 462 (2018) 760–771

[36] K. Jing , W. Ma , Y. Ren , J. Xiong, B. Guoa, Y. Song, S. Liang, L. Wu, Hierarchical Bi_2MoO_6 spheres in situ assembled by monolayer nanosheets toward photocatalytic selective oxidation of benzyl alcohol, Appl. Catal., B 243 (2019) 10–18.

[37] X.F. Zhang , Z. Wang , Y. Zhong , J. Qiu , X. Zhang, Y. Gao , X. Gu, J. Yao, TiO_2 nanorods loaded with Au-Pt alloy nanoparticles for the photocatalytic oxidation of benzyl alcohol, J. Phys. Chem. Solids 126 (2019) 27–32.

[38] H. Huang, H. Yuan, K.P.F. Janssen, G. Solis-Fernandez, Y. Wang, C.Y.X. Tan, D.Jonckheere, E. Debroye, J. Long, J. Hendrix, J. Hofkens, J.A. Steele, M. B. J. Roeffaers, Efficient and selective photocatalytic oxidation of benzylic alcohols with hybrid organic-inorganic perovskite materials, ACS Energy Lett. 3 (2018) 755−759.

[39] A. Ziarati, A. Badiei, R. Luque, Engineered bi-functional hydrophilic/hydrophobic yolk@shell architectures: A rational strategy for non-time dependent ultra selective photocatalytic oxidation, Appl. Catal., B 240 (2019) 72–78.

[40] J. Ding, W. Xu, H. Wan, D. Yuan, C. Chen, L. Wang, G. Guan, W.L. Dai, Nitrogen vacancy engineered graphitic C_3N_4-based polymers for photocatalytic oxidation of aromatic alcohols to aldehydes, Appl. Catal., B 221 (2018) 626–634.

[41] J. Qiu, X. Zhang, K. Xie, X.F. Zhang, Y. Feng, M. Jia, J. Yao, Noble metal nanoparticle-functionalized Zr-metal organic frameworks with excellent photocatalytic performance, J. Colloid Interface Sci. 538 (2019) 569-577.

[42] B. Paul, D.D. Purkayastha, S.S. Dhar, Size-controlled synthesis of $NiFe_2O_4$ nanospheres via a PEG assisted hydrothermal route and their catalytic properties in oxidation of alcohols by periodic acid, Appl. Surf. Sci. 370 (2016) 469–475.

[43] Y. Liu, B. Liua, Q. Wang, C. Lia, W. Hu, Y. Liu, P. Jing, W. Zhaoa, J. Zhang, Three-dimensionally ordered macroporous Au/CeO_2–Co_3O_4 catalysts with mesoporous walls for enhanced CO preferential oxidation in H_2-rich gases, J. Catal. 296 (2012) 65-76.

[44] D.S. Patil, S.A. Pawar, J.C. Shin, Alteration of Ag nanowires to Ag/Ag_2S nanowires@CdS core-shell architectures for electrochemical supercapacitors, J. Alloys Compd. 768 (2018) 1076-1082.

[44] G. Marci, E.I. Garcia-Lopez, L. Palmisano, Polymeric carbon nitride (C_3N_4) as heterogeneous photocatalyst for selective oxidation of alcohols to aldehydes, Catal. Today 315 (2018) 126-137.

Figures and captions

Fig. 1. XRD patterns of (a) 0.5% Ag/Co_3O_4, (b) 1% Ag/Co_3O_4, (c) 1.5% Ag/Co_3O_4, (e) 1 % Ag/Co_3O_4 (spent catalyst).(*-Ag(111)).

Fig. 2. SEM images of the (a,b) fresh (c) spent and (d) SEM-EDS mapping of 1% Ag/Co_3O_4 nanoparticles.

Fig. 3. Elemental mapping of 1% Ag/Co_3O_4 catalyst (a) Ag, (b) Co and (c) O.

Fig. 4. (a, b) TEM images, (c) HRTEM image (lattice fringes) and (d) ED pattern of 1% Ag/Co_3O_4 nanoparticles.

Fig. 5. XPS spectra of (a) Co 2p, (b) O 1s, and (c) Ag 3d spectrum of 1% Ag/Co_3O_4 catalyst.

Fig. 6. (a) N_2 adsorption-desorption isotherm and (b) pore size distribution curve of 1% Ag/Co_3O_4 nanoparticles with different loading.

Fig. 7. FTIR diagram of (a) uncalcined and (c) calcined 1% Ag/Co_3O_4 nanoparticles.

Fig. 8. TGA/DTA analyses of the uncalcined 1% Ag/Co_3O_4 nanoparticles.

Fig. 9. Recyclability test of 1% Ag/Co_3O_4 nanoparticles.

Scheme 1. The possible mechanism for photocatalytic oxidation of aromatic alcohols.

Table 1. Textural properties of 1% Ag/Co_3O_4.

Table 2. Optimization table for photocatalytic oxidation of benzyl alcohol in presence

of 1% Ag/Co_3O_4 catalyst .

Table 3. Activities of the different catalysts for photocatalytic oxidation of benzyl alcohols.

Table 4. Activities of 1% Ag/Co_3O_4 nanostructure catalyst for photocatalytic oxidation of substituted alcohols.

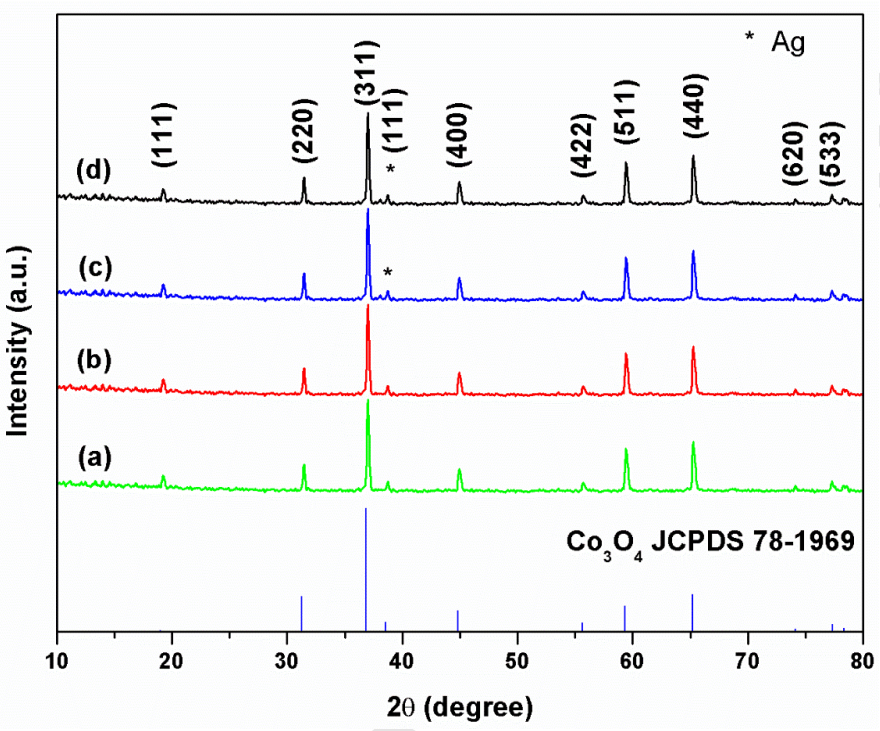

<Fig. 1>

ACCEPTED MANUSCRIPT

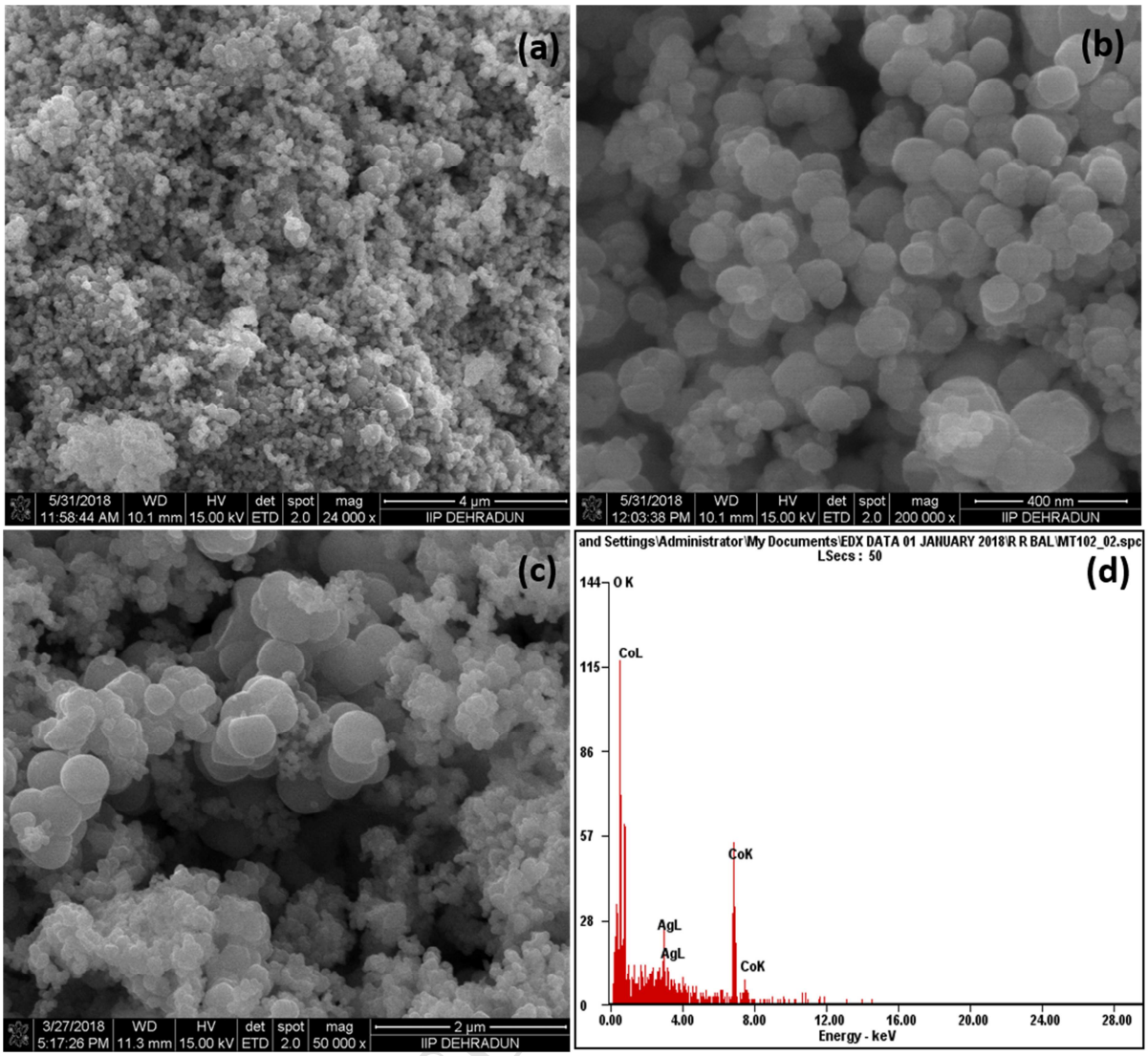
(a)
5/31/2018 WD HV det spot mag 4 µm
11:58:44 AM 10.1 mm 15.00 kV ETD 2.0 24 000 x IIP DEHRADUN
(b)
5/31/2018 WD HV det spot mag 400 nm
12:03:38 PM 10.1 mm 15.00 kV ETD 2.0 200 000 x IIP DEHRADUN
(c)
3/27/2018 WD HV det spot mag 2 µm
5:17:26 PM 11.3 mm 15.00 kV ETD 2.0 50 000 x IIP DEHRADUN
and Settings\Administrator\My Documents\EDX DATA 01 JANUARY 2018\R R BAL\MT102_02.spc
LSecs : 50
(d)
O K
CoL
AgL
AgL
CoK
CoK
144
115
86
57
28
0
0.00
4.00
8.00
12.00
16.00
20.00
24.00
28.00
Energy - keV

<Fig. 2>

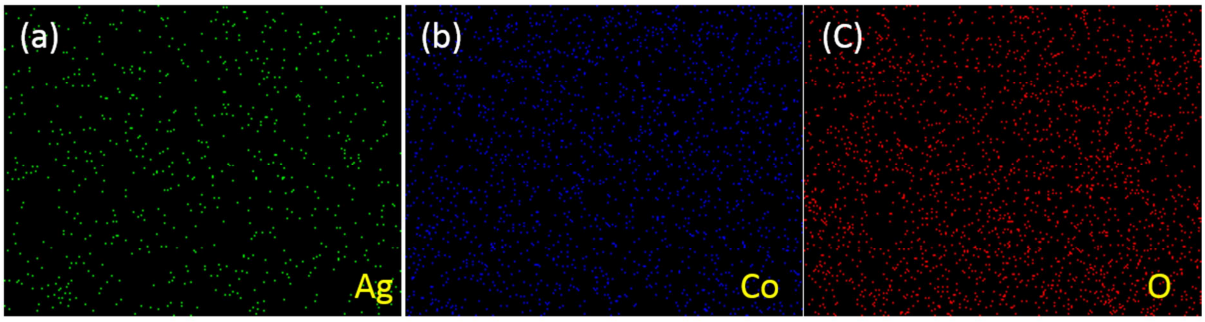
(a)
Ag
(b)
Co
(C)
O

<Fig. 3>

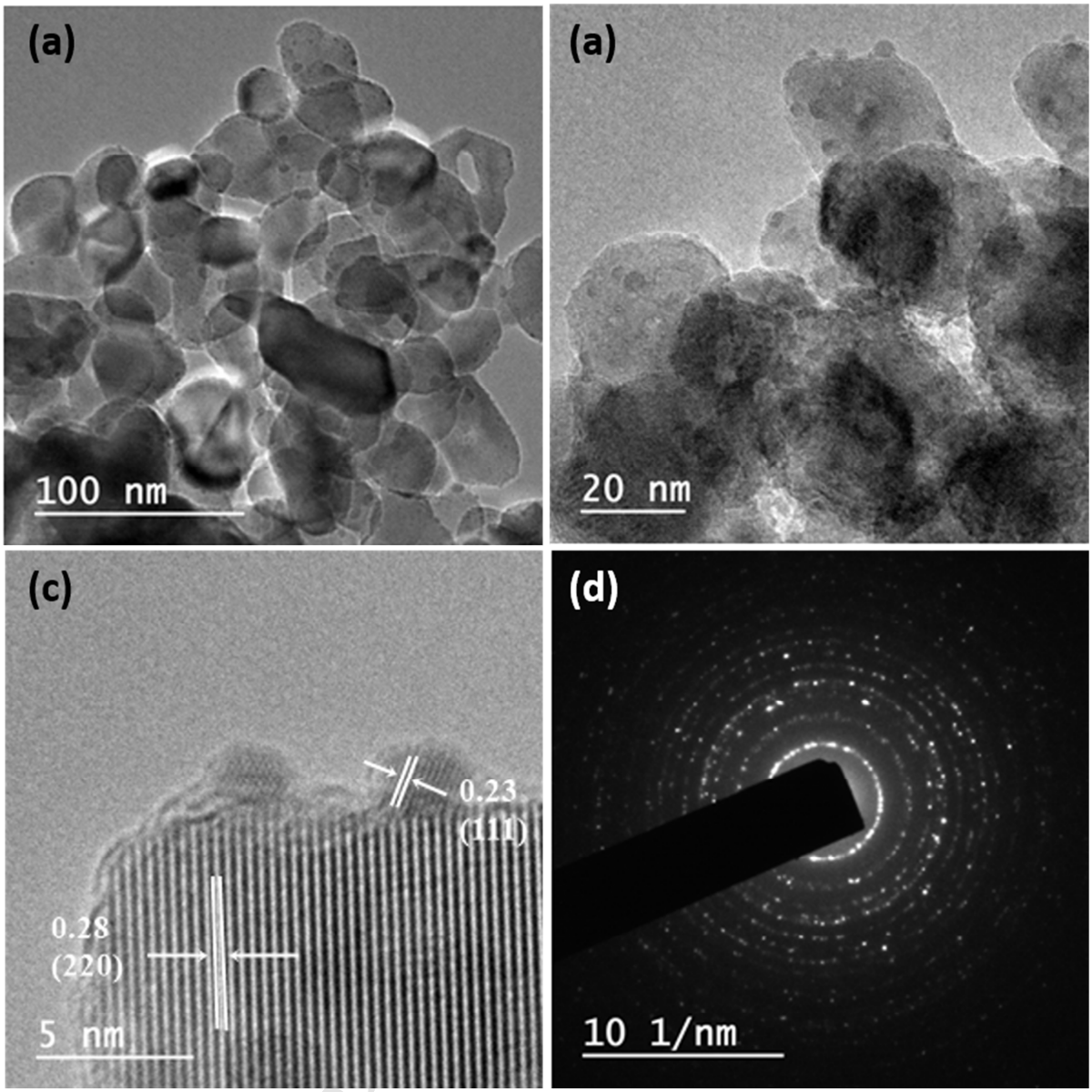
(a)
100 nm
(a)
20 nm
(c)
0.23
(111)
0.28
(220)
5 nm
(d)
10 1/nm

<Fig. 4>

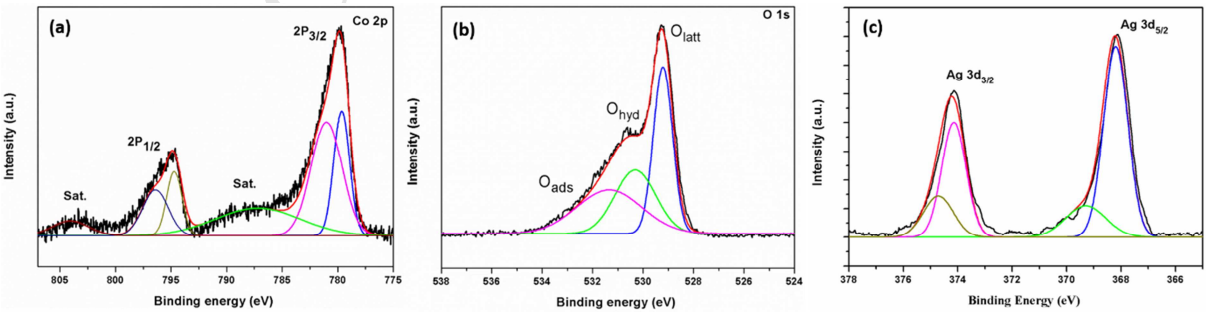
(a)
Co 2p
2P3/2
2P1/2
Sat.
Sat.
Intensity (a.u.)
Binding energy (eV)
(b)
O 1s
Olatt
Ohyd
Oads
Intensity (a.u.)
Binding energy (eV)
(c)
Ag 3d5/2
Ag 3d3/2
Intensity (a.u.)
Binding Energy (eV)

<Fig. 5>

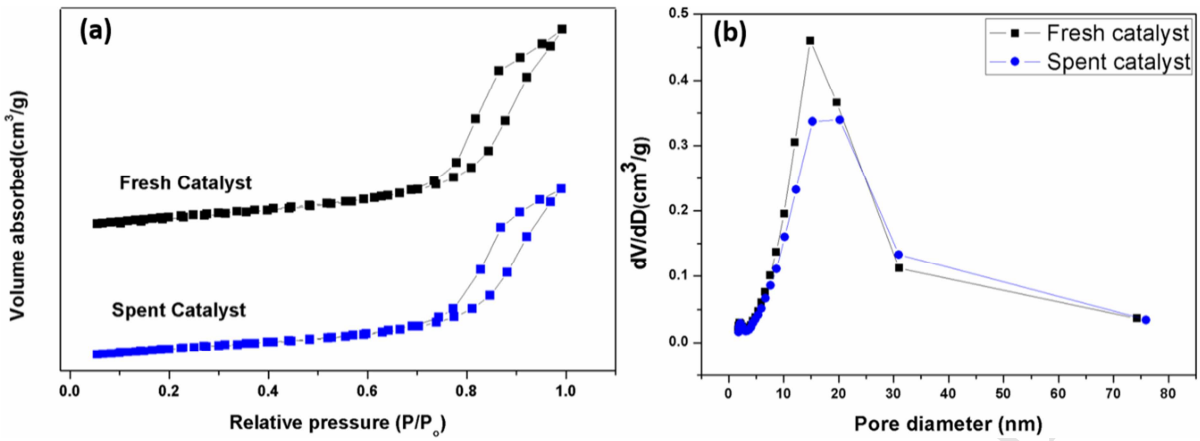
(a)
Fresh Catalyst
Spent Catalyst
Volume absorbed(cm3/g)
Relative pressure (P/Po)
(b)
Fresh catalyst
Spent catalyst
dV/dD(cm3/g)
Pore diameter (nm)

<Fig. 6>

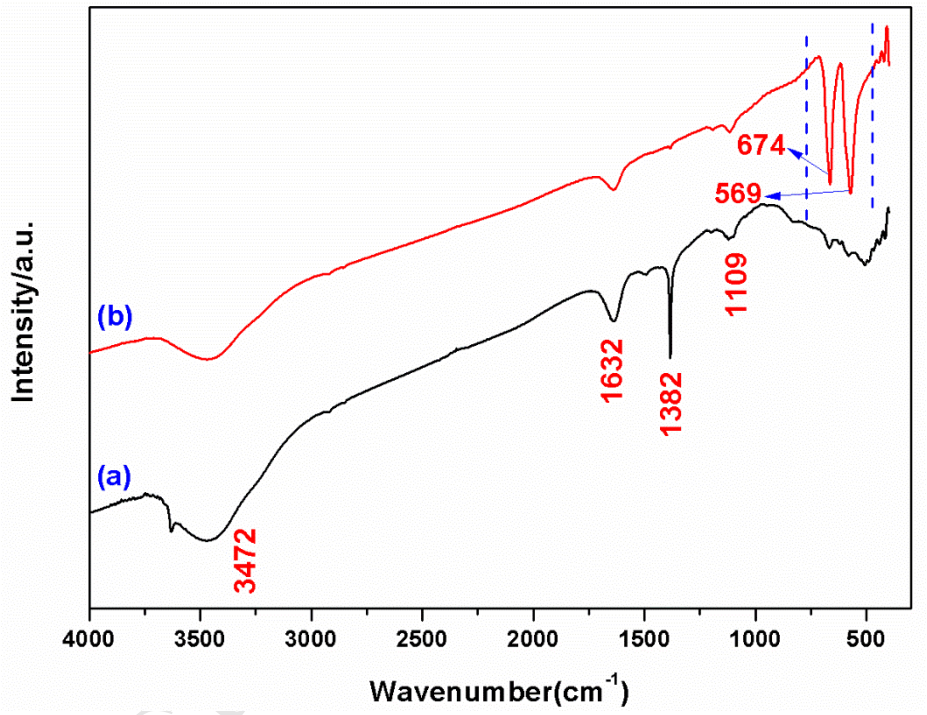
674
569
1109
1632
1382
3472
(b)
(a)
Intensity/a.u.
Wavenumber(cm-1)

<Fig. 7>

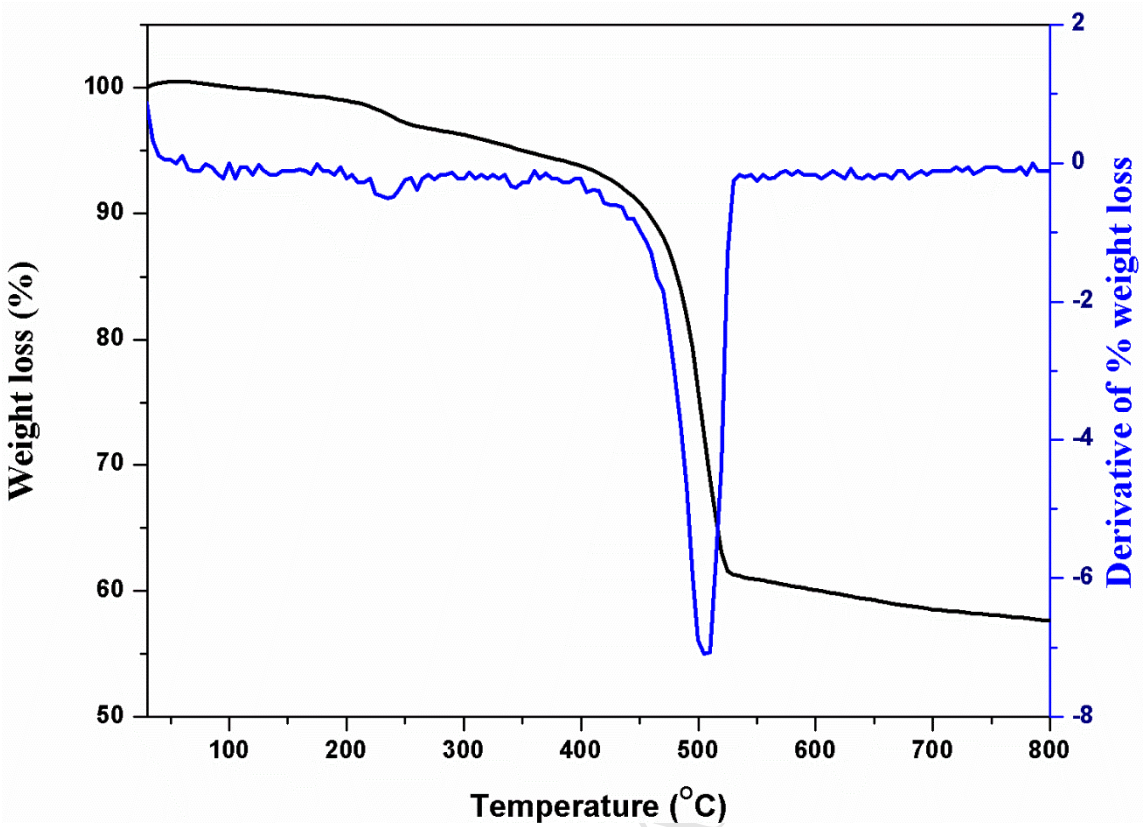
Weight loss (%)
Derivative of % weight loss
Temperature (°C)
100
90
80
70
60
50
2
0
-2
-4
-6
-8
100
200
300
400
500
600
700
800

<Fig. 8>

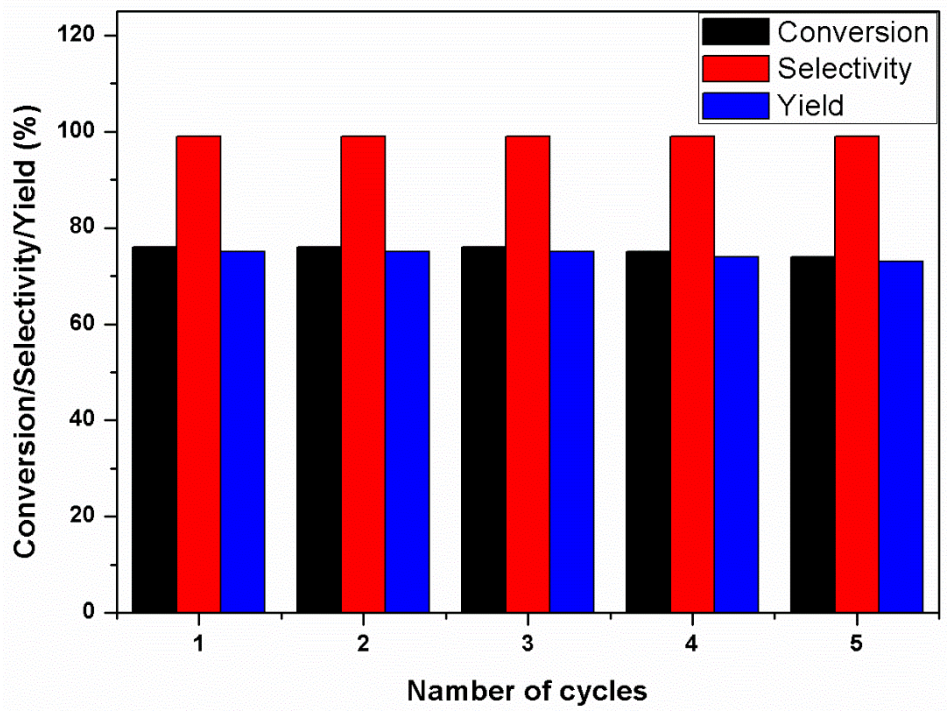
Conversion
Selectivity
Yield
Conversion/Selectivity/Yield (%)
Namber of cycles
120
100
80
60
40
20
0
1
2
3
4
5

<Fig. 9>

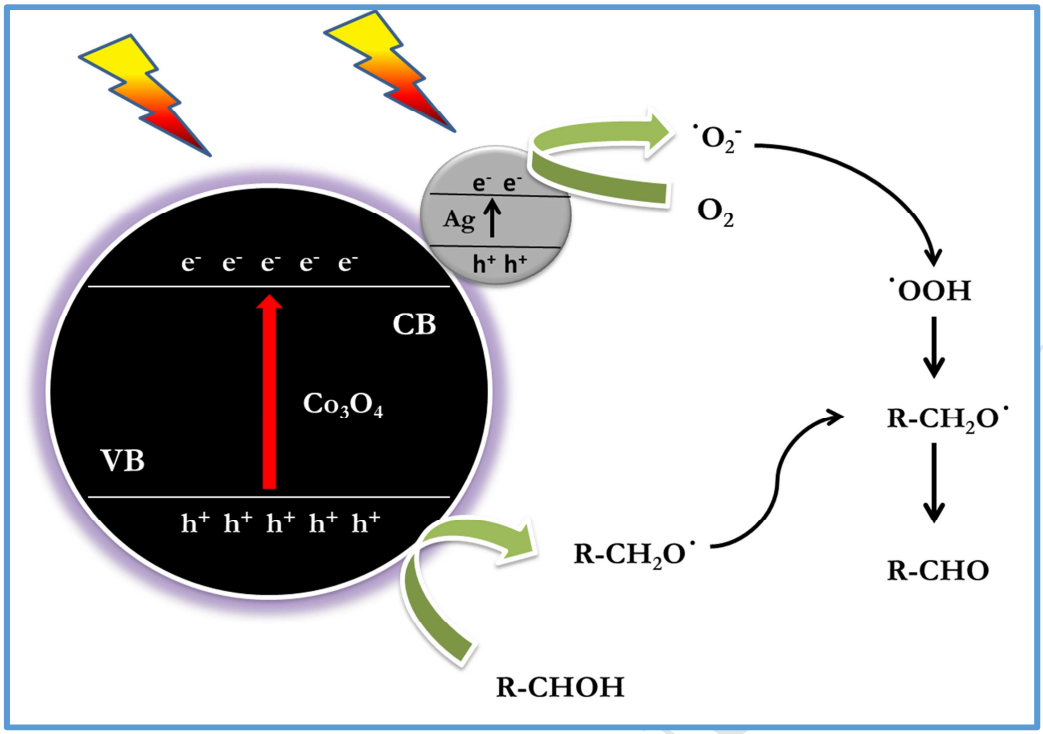

<Scheme 1>

Table 1

Catalyst (Ag/Co_3O_4)	Ag loading	BET specific surface area (m^2/g)	Pore Volume[a] (cm^3/g)	Pore size[b] (nm)
Fresh catalyst	0.9	46.23	0.13	14.1
Spent catalyst	0.8	40.74	0.11	14.6

[a] Total pore volume. [b] Average pore diameter

1 **Table 2**

Entry	Catalyst (mg)	Time (h)	Solvent	Conversion (%)	Selectivity (%)
1	10	12	Acetonitrile	60	99
2	15	12	Acetonitrile	74	99
3	**20**	**8**	**Acetonitrile**	**76**	>99
4	20	4	Acetonitrile	58	>99
5	20	12	Acetonitrile	78	99
6	30	8	Acetonitrile	79	>99
7	20	8	trifluorotoluene	49	>99
8	20	12	dimethyl carbonate	76	97
9	20	8	tributyl phosphate	94	32
10	20	8	Water	28	16
11	-	8	Acetonitrile	8	-

2

3 **Table 3**

Entry	Catalyst	Conversion (%)	Selectivity (%)	Yield (%)
	Ag^{com}	23	96	22
2	Co_3O_4 ^{com}	34	94	32
3	Ag^{us}	27	96	26
4	Co_3O_4 ^{us}	42	95	40
5	$Ag/Co_3O_4^{imp}$	46	96	44
6	1% Ag/Co_3O_4 nano catalyst[e]	76	>99	75
7	1% Ag/Co_3O_4 nano catalyst[f]	74	>99	73
8	0.5% Ag/Co_3O_4	54	>99	53
9	1.5% Ag/Co_3O_4	78	98	76
10	No Catalyst	8	-	-

Conversion of benzyl alcohol based upon the FID-GC results = [moles of benzyl alcohol reacted/initial moles of benzyl alcohol used] × 100. Selectivity of the product calculated by total moles of the product formed/total moles of benzyl alcohol converted; Yield of aldehyde = conversion × selectivity/100;. [e]Fresh catalyst. [f] Spent Catalyst; com = commercial; us = bare Ag and Co_3O_4 prepared by our method; imp = impregnation method.

4

5

6

Table 4

Entry	Substrate	Product	Time (h)	Conversion (%)	Selectivity (%)
1	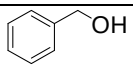	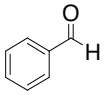	8	76	>99
2	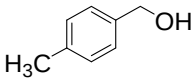	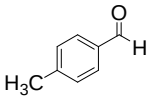	6	76	>99
3	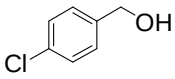	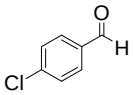	9	75	>98
4	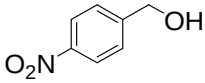	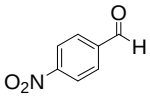	6	78	>99
5	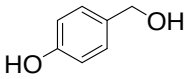	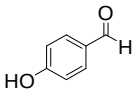	10	74	>99
6	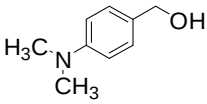	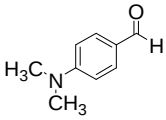	8	76	>99
7	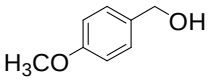	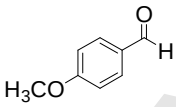	4	78	>98
8	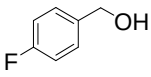	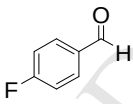	9	75	>98
9	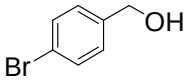	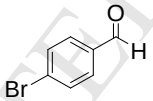	12	72	>98
10	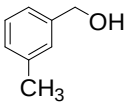	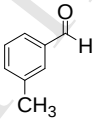	8	78	>99
11	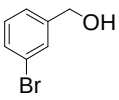	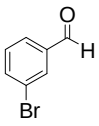	10	76	>99
12	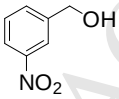	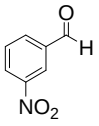	6	79	>99
13	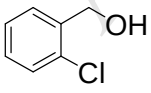	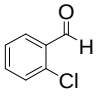	8	75	>99

ACCEPTED MANUSCRIPT

ACCEPTED MANUSCRIPT

Highlights

- One-pot hydrothermal synthesis of silver supported cobalt oxide.
- 2–5 nm Ag-nanoparticles supported on 40–60 nm Co_3O_4 nanosphere.
- Room temperature photocatalytic oxidation of alcohol to aldehyde.
- Alcohol conversion of 76% with 99% selectivity of aldehyde.

ACCEPTED MANUSCRIPT